JOURNAL OF SPACECRAFT AND ROCKETS
Vol. 39, No. 2, March–April 2002

Condition Monitoring of Filament-Wound Composite Flywheels Having Circumferential Cracks

Fuh-Wen Shiue,* George A. Lesieutre,† and Charles E. Bakis‡
Pennsylvania State University, University Park, Pennsylvania 16802

A condition monitoring technique for advanced composite flywheels is presented. Flaws of primary interest, such as delamination and debonding of interfaces, are those unique to filament-wound composite flywheels. Such flaws change the balance state of a flywheel through small but detectable motion of the mass center and principal axes of inertia. The proposed technique determines the existence and the severity of such flaws by a method similar to the influence-coefficient rotor balancing method. Because of the speed dependence of the imbalance caused by elastic flaws, a normalized imbalance change is defined. The normalized imbalance change not only permits the use of vibration readings at multiple speeds to increase the technique's accuracy, but also is a direct measure of the flaw severity. To account for the possibility that flaw growth could actually improve the balance state of a rotor, a new concept of accumulated imbalance change is also introduced. Laboratory tests show the proposed method is able to detect small simulated flaws that result in as little as 2–3 μm of mass center movement. A virtual containment system, which is a condition monitoring system plus additional logic to adjust the flywheel speed when a flaw is detected, was also demonstrated.

Nomenclature

$\boldsymbol{A}$	=	influence coefficient matrix
A_{ij}	=	entry in the ith row, jth column of matrix $\boldsymbol{A}$
e_u	=	mass center offset (eccentricity)
F	=	centrifugal force
k	=	number of sensors
l_u	=	axial distance from location of imbalance to the center of a cylindrical rotor
l_1	=	axial distance from location of mass addition to first balancing plane
l_2	=	axial distance from location of mass addition to second balancing plane
M	=	total mass of a rotor
m	=	number of measurements
m_u	=	unbalance mass addition
n	=	number of balancing planes
q	=	number of speeds at which measurements are taken
R	=	radial location of a flaw
$U, \boldsymbol{U}$	=	single imbalance, imbalance vector
U_a	=	added single imbalance in the flaw growth simulation test
U_d	=	detected imbalance due to mass loss
U_j	=	imbalance added to the jth balancing plane
$Z, \boldsymbol{Z}$	=	vibration measurement, vibration vector
$Z_{i,j}$	=	vibration of the ith sensor with imbalance added at the jth balancing plane
$Z_{i,0}$	=	baseline vibration of the ith sensor
Z_0	=	residual vibration not related to imbalance
ΔU	=	imbalance change
ΔU_N	=	normalized imbalance change
ΔZ	=	vibration change
ΔZ_N	=	normalized vibration change
ω	=	rotation speed

Presented as Paper 2001-1441 at the 42nd Structures, Structural Dynamics, and Materials Conference, Seattle, WA, 16–19 April 2001; received 23 May 2001; revision received 16 November 2001; accepted for publication 18 November 2001.

*Ph.D. Candidate, Department of Aerospace Engineering. Member AIAA.
†Professor, Department of Aerospace Engineering. Associate Fellow AIAA.
‡Professor, Department of Engineering Science and Mechanics.

Introduction

ADVANCED composite flywheels have great potential for use in energy storage systems.[1,2] A typical energy storage flywheel system consists of a composite rotor, a motor/generator, bearings, and, in some cases, a shaft. The electrical energy is applied to the flywheel and stored in the form of rotational kinetic energy. The high specific energy (stored energy per unit weight), fast charge/discharge rate, deeper depth of discharge, less scheduled maintenance, temperature insensitivity, and longer service life give composite flywheels some advantages in competing with alternatives such as electrochemical batteries.

The possible dual functionality of flywheel batteries is also attracting growing interest in spacecraft applications.[3,4] If the angular momentum control devices commonly used in spacecraft attitude control can be used simultaneously for energy storage in place of chemical batteries, significant weight savings can potentially be realized.

A flywheel battery usually operates at very high speed. Because of the possibility of catastrophic failure, burst containment is necessary for most ground-based flywheel systems. A heavy containment system, however, would greatly reduce any advantage in weight for spacecraft applications. Alternatively, an integral health monitoring and virtual containment subsystem is desirable, especially for more rapid acceptance of such a combined energy–momentum storage system. The virtual containment concept uses sensors to monitor changes in a flywheel's operating condition, to estimate the severity if the change is due to flaws, and then to adjust the operating condition accordingly to avoid further flaw growth or system failure.

As in most high-speed rotating machinery, there are several flaw types that could occur in flywheel systems, such as worn bearings and bowed/cracked shafts. Many related issues have been addressed by numerous researchers.[5–9] The types of faults that are unique to composite flywheels, progressive damage (e.g., delamination of composite, debond between rim and hub), have not yet been examined. This study focuses on developing a scheme to identify delaminations and debonds in a filament-wound composite rotor.

Vibration measurements have been used widely in machinery condition monitoring. Various vibration standards for turbomachinery are available in the literature.[10,11] Such standards are established using existing data or previous experience with similar machines of the same scale. The standards only give vibration severity; no information is given on the cause of the vibration and the flaw severity.

Also, existing standards are based on data mostly from metallic rotors; it is not appropriate to apply them directly to composite flywheels.

Depending on the design and manufacturing method for composite flywheels, circumferential delaminations or debonds could be more likely to occur than other composite flaws. Delaminations or debonds change the mass distribution of a rotating flywheel, thus affecting its balance state. The vibration signature for a flawed flywheel at a single speed is the same as that for a rotor with a mass imbalance. Instead of using a vibration signal directly, the severity of rotor flaws can be better estimated by monitoring the balance state of a flywheel system.

Flaws: Elastic Imbalances

As a circumferential flaw initiates and grows on a rotating flywheel rotor, the rotor deforms differently due to the flaw. The nonuniform deformation causes mass redistribution and, hence, moves the system's center of mass away from its original location, that is, it changes the balance state of the rotor. Measuring mass center motion experimentally requires intentionally implementing a flaw on a flywheel during the manufacturing process and spinning the flawed flywheel at high speed. Such a spin test is not only costly, but also dangerous because of the possibility of catastrophic failure. Instead, the finite element method (FEM) was used to investigate the relationship between flaw sizes and the induced imbalances.

Because flywheel rotor and hub designs can vary depending on the applications, the procedure and results described in this section serve as a general guideline. An analogous procedure and analysis must be repeated for different rotor/hub designs of interest, as well as for different flaw types.

Two-dimensional finite element analysis was performed using the commercial FEM code ABAQUS. Figure 1 shows the mesh used in the simple example. The model rotor includes a filament-wound T-1000 carbon/epoxy rim (o.d. = 200 mm) and a solid aluminum hub (o.d. = 80 mm). Second-order, plane stress elements (eight-node quadratic for the composite rim and six-node triangular for the aluminum hub) were used in this example to better model the curvature of the flywheel and to reduce the total number of elements used. The mesh was generated to be as axisymmetric as possible to minimize the numerical value of the initial mass center offset.

Circumferential flaws of various sizes were introduced at different radial locations. A crack was modeled by disconnecting initially collocated nodes of neighboring elements. A through-the-thickness delamination or debond was assumed. Figure 2a shows the mass center motion at three different speeds, with a variable-sized delamination at a radius of 70 mm in the composite rim. Note that imbalance is the product of mass center offset and the total mass of the rotor and has units of mass times distance.

Unlike the common definition of mass imbalance used in rotor balancing, the imbalance created by a fixed-size flaw is not constant. Simple observation shows that it increases with speed squared, or centrifugal force: A circumferential crack is like an elastic imbalance.

Let the normalized imbalance change ΔU_N be defined as the imbalance change divided by the speed squared:

$$\Delta U_N = \Delta U/\omega^2 \tag{1}$$

The normalized imbalance change is independent of speed and is a function of the size and radial location of a flaw. Figure 2b is the same as Fig. 2a, except that the vertical axis is expressed in terms of ΔU_N. The speed independence of ΔU_N is clearly seen in Fig. 2b. For flaws at a certain radial location, the normalized imbalance change increases with the flaw size, up to 180 deg. When a flaw grows over 180 deg, the imbalance change decreases with crack size, that is, the balance state is improved. Evidently, ΔU_N is a good direct flaw-size measure of a single crack smaller than 180 deg. Because a bigger flaw is generally considered more critical, ΔU_N is a possible measure of flaw severity.

The effect of flaw radial location was also studied. Figure 3 shows the normalized imbalance change with respect to the flaw location

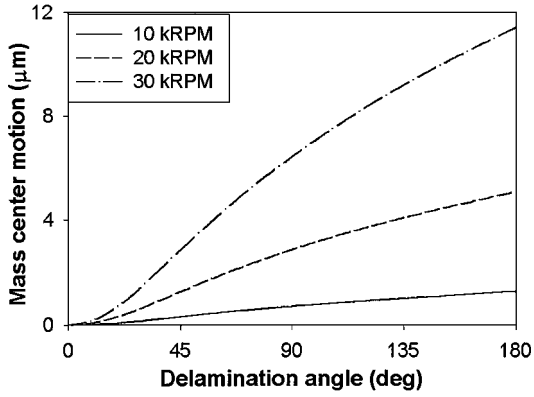

a) Mass center motion

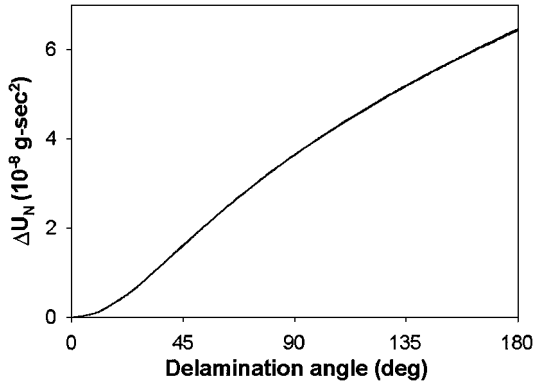

b) Normalized imbalance change

Fig. 2 Delamination at radius of 70 mm.

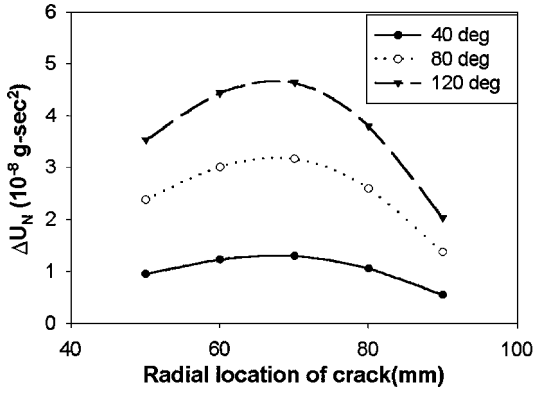

Fig. 3 Normalized imbalance change for flaws at different radial locations in composite rim.

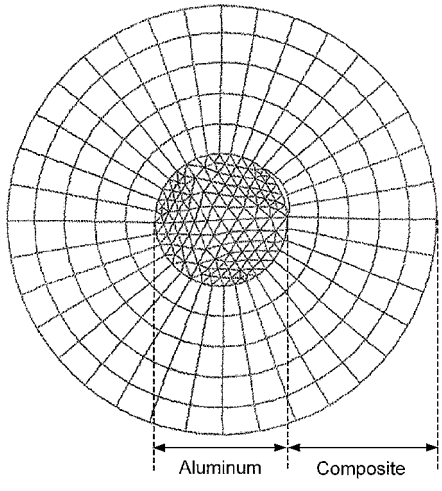

Fig. 1 FE mesh used for flaw simulation.

(in composite rim), for three different flaw sizes. Note that the shape of these curves is similar to that of the radial stress distribution in the composite rim. A circumferential crack of a certain size (angle) at the location of the maximum radial stress evidently creates the largest imbalance change.

Theory

Because the imbalance change is closely related to flaw size, as shown in the preceding section, monitoring the balance state is a good way to assess the condition of a flywheel system. Instead of using vibration measurements alone, monitoring the imbalance change can provide more details about the size of a flaw and, hence, the flaw severity.

Estimating the imbalance change of a flywheel is very similar to the practice of rotor balancing. There are generally two categories of balancing techniques: the influence coefficient method and the modal balancing method. The imbalance monitoring technique adopted in this study is based on the influence coefficient method, which is briefly described.

Imbalances

Consider a perfect disk of mass M, with mass center at the geometric center (Fig. 4).[12] If a small mass m_u ($m_u \ll M$) is added to the disk at radius R, the imbalance U is defined as

$$\boldsymbol{U} = m_u \boldsymbol{R} \tag{2}$$

The mass center offset is often referred to as the rotor unbalance eccentricity e_u. The relation between U and e_u is

$$\boldsymbol{e}_u = m_u \boldsymbol{R}/(M + m_u) = \boldsymbol{U}/(M + m_u) \approx \boldsymbol{U}/M \tag{3}$$

For the ease of manipulation, vectors ($\boldsymbol{R}$, $\boldsymbol{U}$, and $\boldsymbol{e}_u$) are expressed in polar coordinates using complex numbers.

There are two types of imbalances for rigid rotors: static and dynamic. Static imbalance represents the mass center offset from the rotation axis, that is, unbalance eccentricity, which in turn exerts a centrifugal force F on the rotor (Fig. 5a). Dynamic imbalance, on the other hand, does not change the overall mass center location of a rotor, but generates a transverse unbalance moment about the mass center of the rotor (Fig. 5b). This is equivalent to having the spin axis not aligned with a principal axis of inertia. A dynamic imbalance can be replaced by two equal but opposite-phase static imbalances at two different planes along the spin axis.[12]

For a two-dimensional disk rotor, only the mass center offset is required to quantify the state of balance, that is, one imbalance at one plane is sufficient. For a long, cylindrical rotor, both the mass center and the principal axes could shift due to the existence of a flaw. At least two imbalances at two different planes are required to characterize the balance state of a cylindrical rotor.

If a circumferential flaw exists at some axial location in a long flywheel, the imbalance created by this flaw is local. This situation is similar to that obtained by adding a mass imbalance to the original perfect flywheel at that location. Figure 6 shows a rigid rotor with an imbalance U situated at an axial distance l_u from the mass center.

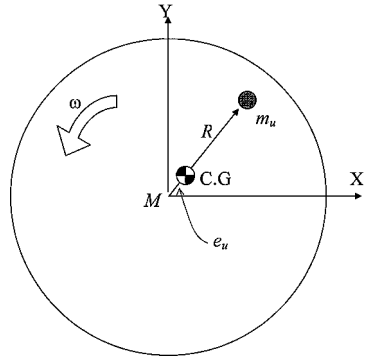

Fig. 4 Single imbalance.

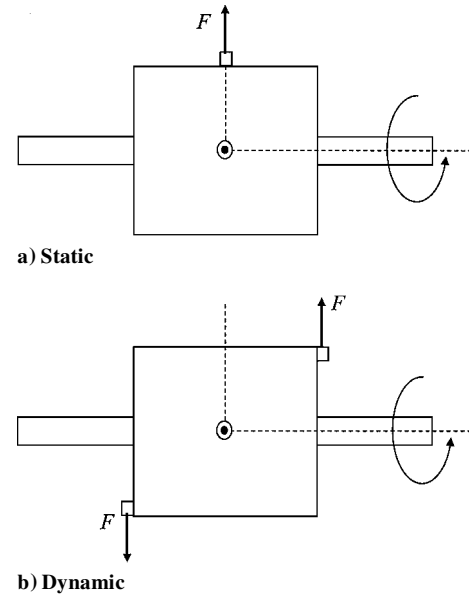

Fig. 5 Imbalance.

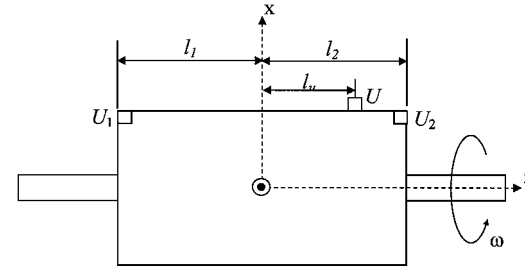

Fig. 6 Rigid rotor with arbitrary imbalance.

The single imbalance can be resolved into two imbalances on two planes according to the following relations:

$$U_1 = U[(l_2 - l_u)/(l_1 + l_2)] \tag{4a}$$

$$U_2 = U[(l_u + l_1)/(l_1 + l_2)] \tag{4b}$$

Note that the two imbalances are in the same azimuthal plane.

Influence Coefficient Method

The basis for the influence coefficient method is straightforward.[12–14] This method requires no advance knowledge of a rotor's dynamic behavior, which makes it very suitable for field balancing applications. The influence coefficient method assumes a linear input–output relation between the imbalance $\boldsymbol{U}$ and the vibration measurement $\boldsymbol{Z}$. This relation can be expressed as

$$\{\boldsymbol{Z}(\omega)\}_{m\times 1} = [\boldsymbol{A}(\omega)]_{m\times n}\{\boldsymbol{U}\}_{n\times 1} \tag{5}$$

Both the imbalance and the vibration measurement are vectors expressed in complex form that contain amplitude and phase information. The entries in matrix $\boldsymbol{A}$ are called influence coefficients, and they vary with rotational speed. An influence coefficient represents the transverse response of a rotor at one axial location to a unit imbalance at another plane for a given speed.

The entries in the influence coefficient matrix $\boldsymbol{A}$ can be determined experimentally by successively adding known masses, called trial masses, to different balancing planes. Before adding any trial mass, the rotor is spun to a specific speed, and the baseline vibrations $\boldsymbol{Z}_0$ are recorded. When a trial mass is attached to the jth balancing plane, the corresponding imbalance addition is denoted as U_j. The rotor is then spun up to the same speed as the initial run, and the vibrations are again recorded. For the next run, the old trial mass is removed, and a new trial mass is added to another balancing plane. The same procedure is repeated until trial masses have been added

to all balancing planes. The entries in the $\boldsymbol{A}$ matrix can then be easily calculated according to

$$A_{ij} = (Z_{i,j} - Z_{i,0})/U_j \tag{6}$$

where $Z_{i,j}$ is the vibration measurement of the ith sensor with the trial mass added at the jth balancing plane, with $Z_{i,0}$ being the baseline vibration at that sensor. More elaborate procedures for optimizing estimates of influence coefficients may be found in the literature.[13]

If the number of measurements and number of balancing planes are the same, that is, $m = n$, the matrix $\boldsymbol{A}$ is square and can be directly inverted (assuming it is nonsingular). The residual imbalances of the rotor can then be calculated directly from

$$\boldsymbol{U} = \boldsymbol{A}^{-1}\boldsymbol{Z} \tag{7}$$

This approach is usually referred to as the exact-point balancing method.

Least-Squares Balancing

In principle, the number of measurements only needs to be equal to the number of balancing planes. However, measurement noise and modeling imperfection always makes extra measurements necessary for high-speed operation. If the number of measurements is greater than the number of balancing planes, that is, $m > n$, the matrix $\boldsymbol{A}$ is not square, and the solution can be sought by the least-squares method. When the lengthy derivation is omitted, least-squares balancing is represented by

$$\boldsymbol{U} = (\boldsymbol{A}^*\boldsymbol{A})^{-1}\boldsymbol{A}^*\boldsymbol{Z} \tag{8}$$

where $\boldsymbol{A}^*$ is the Hermitian conjugate of the matrix $\boldsymbol{A}$ (Ref. 15).

The least-squares influence coefficient balancing method has been proven to be very effective by many researchers in many field applications. Besides using more sensors than the number of balancing planes, measurements at multiple speeds can also be used simultaneously to balance a rotor. If there are k sensors along the rotor, and the measurements are taken at q different speeds, then the vector $\boldsymbol{Z}$ has length of $m = kq$. The basic assumption in using Eq. (8) with multispeed measurements is that the imbalance, or the mass center offset (eccentricity), is constant through the applied speed range.

Monitoring Imbalance Using the Influence Coefficient Method

In practice, the relationship between vibration and imbalance is not linear; there are always some extraneous vibrations that are not associated with the imbalance $\boldsymbol{U}$. One example is the vibration caused by bearings. Thus, a more general expression for the influence coefficient method is given as

$$\boldsymbol{Z} = \boldsymbol{A}(\omega)\boldsymbol{U} + \boldsymbol{Z}_0(\omega) \tag{9}$$

where $\boldsymbol{Z}_0$ is the residual vibration that has nothing to do with imbalance. For rotor balancing, correction masses are added to counteract the total vibration, which may result from imbalances as well as other sources such as bearing wear and misalignment. For the purpose of health monitoring of composite flywheels, the focus is on detecting imbalance changes that are due to flaws. When the initial state is subtracted, Eq. (9) can be rewritten as

$$\Delta\boldsymbol{Z} = \boldsymbol{A}(\omega)\Delta\boldsymbol{U} \tag{10}$$

Equation (10) clearly states that the change in imbalance is linear with respect to the change in vibration measurement and is a more accurate statement than the basis of the original influence coefficient method. Equation (10) is also more practical for a health monitoring application.

Because Eq. (10) is similar to Eq. (5), the least-squares solution for Eq. (10) can easily be obtained as follows:

$$\Delta\boldsymbol{U} = (\boldsymbol{A}^*\boldsymbol{A})^{-1}\boldsymbol{A}^*\Delta\boldsymbol{Z} \tag{11}$$

For a cylindrical flywheel, at least two calibration planes are required. Because the balancing plane is where influence coefficients need to be determined, a balancing plane is hereafter called a calibration plane in imbalance monitoring. With two calibration planes, the imbalance created by flaws at arbitrary locations can be detected and expressed in terms of two imbalances, one on each of these two planes, ΔU_1 and ΔU_2 (Fig. 6). If only one flaw is assumed to initiate or grow at a time, the imbalance due to this flaw, ΔU, can be expressed as

$$\Delta\boldsymbol{U} = \Delta\boldsymbol{U}_1 + \Delta\boldsymbol{U}_2 \tag{12}$$

The axial location of this single imbalance can also be determined if the two detected imbalances ΔU_1 and ΔU_2 are in the same azimuthal plane. In practice, however, they usually do not have the same phase. Extensive efforts are needed to localize the axial position of the flaw in such a case and are beyond the scope of this paper.

Note that vibrations caused by imbalances are synchronous, having the same frequency as the rotating speed. In most cases, especially when there is high measurement noise, using a bandpass filter can also improve performance of the proposed method. In this investigation, 1 s of measurements was recorded and processed. To reduce noise, the data were processed using a discrete Fourier transform, and the signal was reconstructed using frequency components in the vicinity of the rotating frequency.

Real Flaws and Simulated Flaws

If $\Delta\boldsymbol{U}$ in Eq. (10) is replaced with the normalized imbalance $\Delta\boldsymbol{U}_N$ for a flaw-induced imbalance, Eq. (10) can be written as

$$\Delta\boldsymbol{Z} = \boldsymbol{A}(\omega)\omega^2\Delta\boldsymbol{U}_N \tag{13}$$

Dividing Eq. (13) by ω^2 yields

$$\Delta\boldsymbol{Z}_N = \boldsymbol{A}(\omega)\Delta\boldsymbol{U}_N \tag{14}$$

where $\Delta\boldsymbol{Z}_N = \{\Delta\boldsymbol{Z}/\omega^2\}$ is defined as the normalized vibration change.

Equation (14) is important for flywheel condition monitoring. It relates a fixed mass imbalance commonly used in rotor balancing to a flaw-induced elastic imbalance and also provides a way to simulate experimentally a delamination-type flaw. For a real flaw, although its size is fixed, the imbalance is speed dependent, that is, the flaw-induced imbalance is not constant. Because the vibration measurements at different speeds actually correspond to different imbalances, the measurements cannot be used simultaneously in the least-squares method as expressed by Eq. (11). When Eq. (14) is used, however, the normalized imbalance change and the normalized vibration change have the same relationship as that of a fixed imbalance and the corresponding vibration change. Because $\Delta\boldsymbol{U}_N$ is constant for a given flaw at all speeds, Eq. (14) yields a relationship similar to Eq. (11):

$$\Delta\boldsymbol{U}_N = [\boldsymbol{A}^*(\omega)\boldsymbol{A}(\omega)]^{-1}\boldsymbol{A}^*(\omega)\Delta\boldsymbol{Z}_N \tag{15}$$

This equation shows that the usual multispeed least-squares method can still be conveniently applied to flaw-induced elastic imbalances, provided that the corresponding normalized quantities $\Delta\boldsymbol{Z}_N$ and $\Delta\boldsymbol{U}_N$ are used. Note that the influence coefficient matrix $\boldsymbol{A}$ in Eq. (15) is the same as that in the regular rotor balancing practice.

Because of the danger and uncertainty of intentionally implanting real flaws in high-speed flywheels, point masses (fixed imbalances) were added to and removed from flywheels during laboratory tests, to simulate real circumferential flaws (elastic imbalances). The similarity between Eqs. (10), (11), (14), and (15) also permits the use of such simulated flaws. For the simulated case, the usual vibration change is used to calculate the fixed imbalance. This is similar to the procedure for rotor balancing. In contrast, the normalized vibration change is needed for estimating the normalized imbalance change, which is constant for a given real flaw. Table 1 compares the approaches for evaluating real and simulated flaws.

Table 1 Approaches for evaluating real and simulated flaws

Approach	Real flaw (delamination)	Simulated flaw (point mass)
Measured quantity	$\Delta \boldsymbol{Z}_N$	$\Delta \boldsymbol{Z}$
Estimated quantity	$\Delta \boldsymbol{U}_N$	$\Delta \boldsymbol{U}$
Equations	$\Delta \boldsymbol{Z}_N = \boldsymbol{A} \Delta \boldsymbol{U}_N$ $\Delta \boldsymbol{U}_N = (\boldsymbol{A}^* \boldsymbol{A})^{-1} \boldsymbol{A}^* \Delta \boldsymbol{Z}_N$	$\Delta \boldsymbol{Z} = \boldsymbol{A} \Delta \boldsymbol{U}$ $\Delta \boldsymbol{U} = (\boldsymbol{A}^* \boldsymbol{A})^{-1} \boldsymbol{A}^* \Delta \boldsymbol{Z}$

Accumulated Imbalance Change

Not all flaws increase vibration levels; some flaws may actually improve the balance state of a flywheel and reduce the vibrations if the flaws occur at locations opposite to the residual imbalance or if a flaw grows over 180 deg. Because the balance state may improve when a flaw initiates, vibration standards alone are not satisfactory for flywheel condition monitoring. To account for the effects of such flaws, a concept for tracking an accumulated imbalance change was developed. The accumulated imbalance change is the sum of the magnitudes of incremental (normalized) imbalance changes that exceed a defined threshold noise level, which may depend on the specific instrumentations and monitoring techniques used. The accumulated imbalance change is a strictly nondecreasing measure of damage accumulation, whereas the absolute imbalance change might not be, as in the case of a delamination growing from 180 to 360 deg.

Experiments and Results

Test Facilities

Two different flywheel systems were used in experiments to validate the proposed condition monitoring technique. Brief descriptions of the test setups are given next.

Flywheel system A has a disklike rotor (Fig. 7) and was used for single-plane imbalance tests. The composite rotor consists of two rings: a carbon/epoxy outer ring and a glass/epoxy inner ring. The rotor (plus a steel hub) weighs about 2 kg and has an o.d. of 17.8 cm and a thickness of 4.8 cm. The rotor is cantilevered from an electric motor that is rated for 10,000 rpm. The flywheel/motor assembly is attached to the ground through four rubber isolation mounts.

A variable number of displacement sensors were mounted on a stationary support and were situated at two planes on the motor to measure vibrations of the flywheel system. These sensors have a resolution of about 1 μm. An infrared tachometer sensor aimed at the shaft measured the speed and also provided a phase reference for the vibration sensors. The sensor signals were recorded by a computer for storage and processing.

Flywheel system B (Fig. 8) is somewhat larger than system A and capable of higher speeds. A cylindrical composite rotor is used in this setup. The rotor is a one-piece carbon/epoxy cylindrical ring, attached to the steel shaft through two solid hubs at top and bottom of the cylinder. Each solid hub has a glass/epoxy outer ring and an aluminum inner hub.

Unlike system A, the shaft of flywheel B is supported at both ends by high-speed ceramic ball bearings on compliant mounts. To achieve high speed and to minimize air drag, the flywheel must be spun in vacuum. The flywheel assembly is spun inside a spin pit, and a high-speed electric motor rated for 35,000 rpm is mounted outside to drive the flywheel. A magnetic clutch is used to transmit torque through the vacuum barrier. The use of a magnetic clutch simplifies sealing of the spin pit. Also, in the event of a flywheel failure, because there is no direct contact of the motor and the flywheel, the chance of damaging the motor is minimized. Two orthogonal displacement sensors were mounted at each bearing of system B to monitor the vibrations of the bearing housings. An optical tachometer monitored speed.

With the high-power/high-speed electrical motor of system B, the displacement sensors were seriously affected by the motor noise. Sharp voltage spikes (about 0.2 V) randomly appear in the sensor measurements. The amount of the voltage spike is equivalent to about 20 μm of displacement noise, which is also in the form of sharp spike. The accuracy of the monitoring method was, therefore, affected by this sensor/motor noise. An upgrade to the instrumentation system is advised if better accuracy is desired.

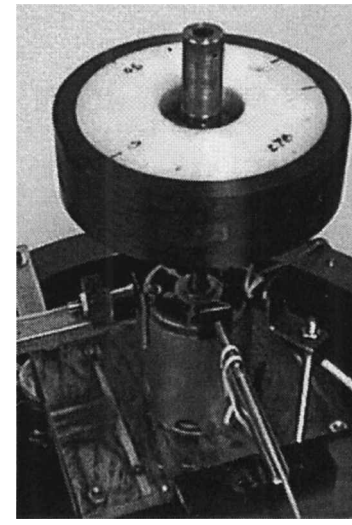

a) Photograph

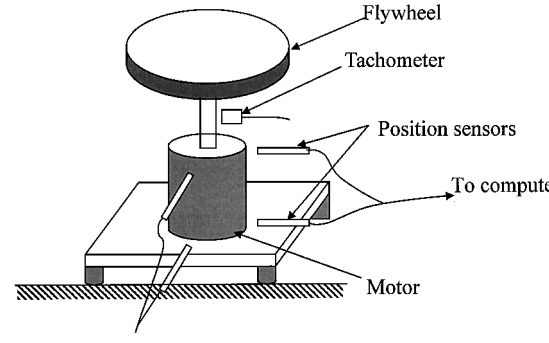

b) Schematic

Fig. 7 Flywheel system A.

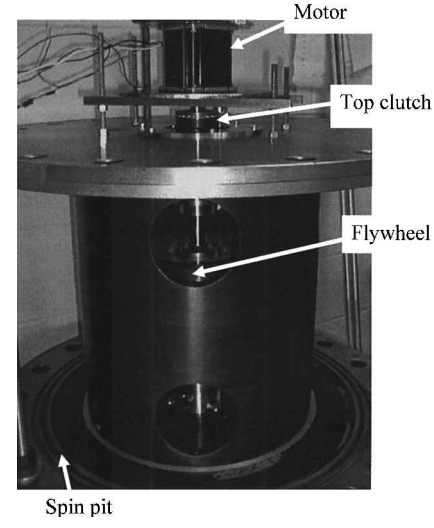

Fig. 8 Flywheel system B.

Balancing is a critical task for high-speed rotating machinery. Both flywheels were well balanced before the tests to ensure smooth operation. The peak vibrations were reduced to less than 10 μm at critical speeds.

Single-Plane Monitoring: Disk Rotor

For monitoring a disklike flywheel, the imbalance on just a single plane is needed. To illustrate and verify the health monitoring concept, initial spin tests were conducted using flywheel A at medium speed.

The flywheel's dynamic response was first characterized, that is, the influence coefficients (as functions of speed) were determined before actual condition monitoring. This process consists of several test runs with and without trial mass attached to the flywheel. Once the influence coefficients are known, the condition monitoring can be performed on the flywheel during operation, in real time.

The rotor (with no mass added) was spun up to 9000 rpm. Vibration measurements were taken at two different speeds (6000 and 9000 rpm). This test is referred to as the reference run herein because it is meant to establish the baseline vibrations in a reference state.

Small pieces of brass were then bonded to the outer surface of the flywheel at different locations, one at a time. The mass of each brass piece was known and created about 10 μm of mass center movement. The flywheel was spun up again, and measurements were taken at 6000 and 9000 rpm. The changes in vibrations were calculated with respect to the reference state and were used to back calculate the imbalances for each mass addition.

Table 2 shows the actual and calculated imbalances for three cases, each with a different number of measurements used in the calculation. Ideally, one sensor reading is sufficient for single-plane imbalance monitoring as suggested by the exact-point influence coefficient method, Eq. (6). With only one sensor measurement at one speed, however, the errors were very large, too large to use the exact-point method in condition monitoring.

Because of the presence of measurement noise and nonlinearity in the system response, a single sensor measurement yields poor results in practice. To reduce errors, more sensors are necessary, and the least-squares balancing method was adopted. With four sensors, two at the top and two at the bottom, the accuracy was greatly improved.

The accuracy can be further improved if more vibration measurements are available, either with more sensors or with the same number of sensors but taking measurements at multiple speeds. Using four sensors and taking data at two speeds (eight measurements total), the results show substantial improvement in the accuracy. With the least-squares method, more independent measurements yields better results.

Table 2 Test results for single-plane monitoring

Added imbalance, g · mm/deg	Detected imbalance, g · mm/deg		
	1 Sensor, 9000 rpm	4 Sensors, 9000 rpm	4 Sensors, 6000 and 9000 rpm
29.3/0	18.9/95	26.1/12	27.5/0
29.1/180	41.0/165	30.8/166	28.4/190
18.1/93	23.2/254	19.6/115	18.0/96

Two-Plane Monitoring: Cylindrical Rotor

Similar tests were performed on flywheel system B. Because flywheel B has a cylindrical rotor, two calibration planes are required. Although the locations of these two planes are not critical, a few practical considerations make some planes more suitable than others. The planes should be far enough apart to ensure that vibration patterns are different when a given mass is added to the different planes. Like the single-plane tests, determination of influence coefficients involves a sequence of tests involving added trial masses. The top and bottom surfaces of the flywheel were chosen as the calibration planes because of easy access.

The experimental procedure for flywheel B was slightly different than that for the single-plane test. After the influence coefficients were determined at various speeds (reference speeds), no reference run was done. A known mass was attached to the outer surface of the flywheel with a piece of adhesive tape. Masses were repeatedly added at different axial locations along the length each time. When the flywheel was spun up to one of the reference speeds, the first set of vibrations was taken as the reference state. Thus, the reference state included the effect of the added imbalance. The flywheel was maintained at that speed until the added mass ejected, and the imbalance changes relative to the reference state were then calculated. A computer program was developed in LabView to automatically perform this task. LabView is a graphical programming language specialized for data acquisition and processing. Programs in LabView are usually called Virtual Instruments (VIs).[16]

Table 3 shows the results for two-plane monitoring tests. The added imbalances shown were quite small indeed. The 25.0 g · mm imbalance corresponds to a mass weighing about 0.19 g attached to

Table 3 Test results for two-plane monitoring

Speed, rpm	Added imbalance, g · mm/deg	Detected imbalance, g · mm/deg
10,250	43.4/0	51.6/1
10,500	50.7/180	58.7/180
11,000	25.0/60	20.8/59

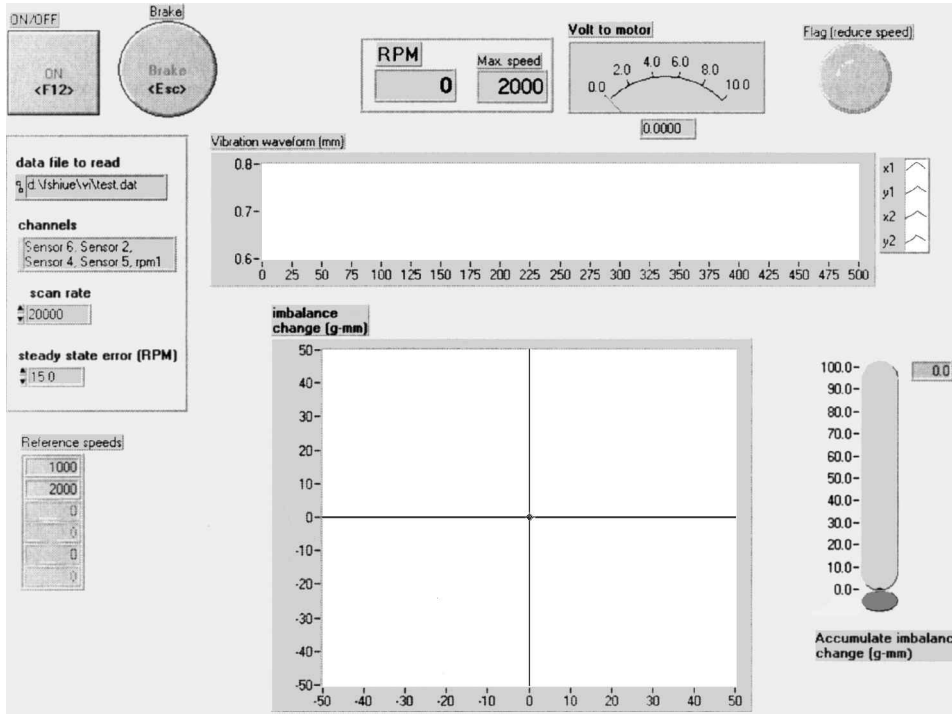

Fig. 9 Front panel of VCVI.

the rim (radius = 134 mm) of the flywheel. This imbalance addition accounts for about 2 ~ 3 μm of mass center movement. The results show excellent phase agreement, whereas the error in magnitude is about 15%. The proposed monitoring method is quite accurate for a cylindrical flywheel and is able to detect small imbalance changes.

Virtual Containment: Flaws Growth Simulation

With the success of the proposed monitoring method, a virtual containment VI (VCVI) was developed (Fig. 9). Virtual containment involves a condition monitoring technique, coupled with a speed control scheme. A maintenance-oriented strategy might lead simply to shutting down the flywheel for maintenance, no matter how minor a flaw is. Such an approach is perhaps acceptable for ground-based applications, but is not desirable for spacecraft applications.

For spacecraft, a better approach would allow a flaw to grow steadily but prevent the flaw from causing catastrophic failure during the flywheel's service life. To determine accurately the severity of a flaw, detailed fracture mechanics analyses of composite flywheels are needed.

Because there was no fracture mechanics analysis at this stage of the research, an alternative approach was adopted. The basic concept is that any change in monitored imbalance for a flywheel system is undesirable and should be avoided. A change in balance state usually indicates flaw growth or initiation. When a change is observed, the maximum speed is gradually reduced by an arbitrary, predetermined amount until no further change occurs.

The condition monitoring scheme described in the preceding sections was the main component of this VCVI. The VCVI constantly monitors the balance state of the flywheel. If an imbalance change exceeds a threshold, the VI automatically reduces the rotational speed by a preset amount (250 rpm in the test). The threshold value was set to 3 μm of mass center motion to account for the detectability with the current setup.

This VCVI was tested in a flaw growth simulation experiment. Flaw growth was simulated by releasing masses from the rotor at different instances during the test. Four different-sized masses were taped to the outer surface of flywheel B at different axial locations before the test (Table 4). The speed was first brought up to and then maintained at 11,000 rpm. After a few minutes, the first mass was ejected. The VI detected the event and slowed the flywheel to the predetermined speed of 10,750 rpm, the next highest reference speed. Subsequent masses were ejected at different times, and the VI further reduced the speed successfully each time.

Figure 10 shows the trace of the mass center movement during the experiment. Note that the mass center is the imbalance divided by

Table 4 Different events during growing flaw simulation test

Event	RPM1[a]	U_a, g · mm/deg	U_d, g · mm/deg	RPM2[b]
1	11,000	39.5/120	51.1/120	10,750
2	10,750	45.9/180	63.6/182	10,500
3	10,500	47.4/0	52.2/−11	10,250
4	10,250	26.5/270	41.2/264	10,000

[a]Initial speed in flow growth simulation test.
[b]Speed target following mass loss in flow growth simulation test.

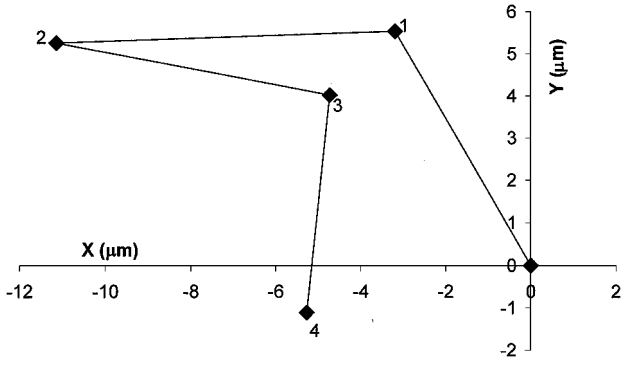

Fig. 10 Mass center movement during flaw growth simulation experiment.

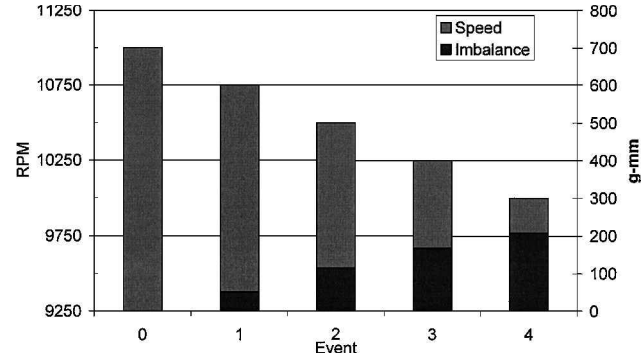

Fig. 11 Speeds and accumulated imbalance changes at different mass loss events during the flaw growth simulation experiment.

the total mass of the flywheel, and the origin of the plot represents the initial mass center of the rotor (rotor plus four masses). The flywheel speeds and the corresponding accumulated (nondecreasing) imbalance changes are plotted in Fig. 11.

Conclusions

The proposed monitoring method, based on multispeed influence coefficients, was shown to be very effective for evaluating the balance state of a flywheel system. Experimental results on both disk-like and cylindrical flywheels demonstrated that imbalance changes (magnitude and phase) can be accurately determined. Mass center movements as small as 2–3 μm were able to be detected.

More independent vibration measurements generally improve the accuracy of measured imbalance changes. These measurements can be achieved by using more sensors or by taking additional measurements at multiple speeds. Improvements are still needed in methods to determine the axial location of imbalance changes. Improved displacement sensors with less electrical noise will also facilitate improvement of the accuracy of the imbalance estimates. Mass center motion equivalent to the sensor resolution (1 μm) should be readily detectable if measurement noise can be reduced.

The notion of accumulated imbalance change, the nondecreasing sum of incremental imbalance changes, is especially useful for monitoring growing and multiple flaws. This accumulated imbalance change is a good measure of overall damage accumulation.

The concept of virtual containment was successfully demonstrated. Virtual containment software (a VCVI) was developed using a relatively simple control approach. In tests using simulated growing flaws, the system successfully reduced the maximum operating speed by a predetermined amount (250 rpm) as increments of imbalance change were detected. To avoid an overly conservative derating of speed with imbalance change using this virtual containment approach, better quantitative estimates of flaw severity and growth rates, perhaps based on fracture mechanics, will be needed.

Acknowledgments

This research was supported by the U.S. Air Force (Contract F29601-98-C-0008) and Applied Material Technologies, Inc. (PO Number 1296). The advice and encouragement of Jerry Fausz and William E. Davis are appreciated.

References

[1]Genta, G., *Kinetic Energy Storage: Theory and Practice of Advanced Flywheel System*, Butterworths, London, 1985, pp. 27, 28.

[2]Proctor, P., "Flywheels Show Promise for 'High-Pulse' Satellite," *Aviation Week and Space Technology*, Jan. 1999, p. 67.

[3]Patel, M. R., "Flywheel Energy Storage for Spacecraft Power Systems," *34th Intersociety Energy Conversion Engineering Conference* [CD-ROM], Society of Automotive Engineers, Warrendale, PA, 1999, SAE Paper 1999-01-2589.

[4]Christopher, D. A., and Donet, C., "Flywheel Technology and Potential Benefits for Aerospace Applications," *IEEE Aerospace Applications Conference Proceedings*, Vol. 1, IEEE Computer Society, Los Alamitos, CA, 1998, pp. 159–166.

[5]Eisenmann, R. C., Sr., and Eisenmann, R. C., Jr., *Machinery Malfunction Diagnosis and Correction: Vibration Analysis and Troubleshooting for*

the Process Industries, Prentice–Hall, Upper Saddle River, NJ, 1998, pp. 395–458.

[6]Edwards, S., Lees, A. W., and Friswell, M. I., "Fault Diagnosis of Rotating Machinery," *Shock and Vibration Digest*, Vol. 30, No. 1, 1998, pp. 4–13.

[7]Scheibel, J. R., Imam, I., Ebben, T. G., and Blomgren, R., "An Expert System-Based, On-Line Rotor Crack Monitor For Utility Steam Turbines," *Proceedings of the 51st American Power Conference*, Vol. 51, Illinois Inst. of Technology, Chicago, 1989, pp. 369–380.

[8]Wu, M. C., and Huang, S. C., "In-Plane Vibration and Crack Detection of a Rotating Shaft-Disk Containing a Transverse Crack," *Journal of Vibration and Acoustics*, Vol. 120, No. 2, 1998, pp. 551–556.

[9]Ratan, S., Baruh, H., and Rodriguez, J., "On-Line Identification and Location of Rotor Cracks," *Journal of Sound and Vibration*, Vol. 194, No. 1, 1996, pp. 67–82.

[10]McHugh, J. D., "Setting Vibration Criteria for Turbomachinery," *Proceedings of the 18th Turbomachinery Symposium*, Texas A&M Univ., College Station, TX, 1989, pp. 127–135.

[11]"ISO 1940-1973, Balance Quality of Rotating Rigid Bodies," *ISO Standards Handbook 4: Acoustics, Vibration and Shock*, 2nd ed., International Organization for Standardization, Geneva, 1985, pp. 654–662.

[12]Gunter, E. J., and Jackson, C., "Balancing of Rigid and Flexible Rotors," *Handbook of Rotordynamics*, edited by F. F. Ehrich, rev. ed., Krieger, Malabar, FL, 1999, pp. 3.1–3.117.

[13]Darlow, M. S., *Balancing of High-Speed Machinery*, Springer-Verlag, New York, 1989, pp. 81–106.

[14]Lund, J. W., and Tonnesen, J., "Analysis and Experiments on Multi-Plane Balancing of a Flexible Rotor," *Journal of Engineering for Industry*, Vol. 94, No. 1, 1972, pp. 233–242.

[15]Goodman, T. P., "A Least-Square Method for Computing Balance Corrections," *Journal of Engineering for Industry*, Vol. 86, No. 3, 1964, pp. 273–279.

[16]"LabView 5.0 User Manual," National Instruments Corp., Austin, TX, Jan. 1998.

R. B. Malla
Associate Editor